Indian Journal of Chemical Technology
Vol. 33, May 2026, pp. 473-484
DOI: 10.56042/ijct.v33i3.17347

Numerical attribution of bioconvection magnetised electrical flow of thermal radiation in a nanoliquid with thermal/solutal convective curve surface

Agha Yasir Ali[1], Syed Sohaib Zafar[2], Farhan Ali[3] *, M. Faizan Ahmed[3], Dana Mohammad Khidhir[4,5] & Hamed Ould Sidi[6]

[1]Department of Applied Computing and Emerging Sciences, Sir Syed University of Engineering and Technology, Karachi, Pakistan

[2]Department of Mathematical Sciences, Sir Syed University of Engineering and Technology, Karachi, Pakistan

[3]Department of Mathematical Sciences, Federal Urdu University of Arts, Sciences & Technology, Gulshan-e-Iqbal, Karachi, 75300, Pakistan

[4]Department of Petroleum Engineering, College of Engineering, Knowledge University, Erbil44001, Iraq

[5]Department of Petroleum Engineering, Al-Kitab University, Altun Kupri, Iraq

[6]Institut Supérieur de Comptabilité et d'Administration des Entreprises- ISCAE, Manouba, Tunisia

*E-mail: farhanali@fuuast.edu.pk

Received 21 February 2025; accepted 12 February 2026

The influence of chemical species on the magnetised bioconvection flow of viscous nanofluid upon a curved surface is scrutinized in this exploration. Additionally, Brownian motion, heat generation/absorption, thermal radiation, and thermophoretic are included. Thermal/solutal, two constraints have been taken to compute the heat and mass transport analysis. To boost the effectiveness of the system, a method describing the viscous nanoliquid behaviour of the stretching curved is revealed by the present research's supplement. The dynamics of constitutive equations are rendered to model the transformation equation via the similarity factor. bvp4c techniques are then considered to solve the model transformation equation. The augmented values of the magnetic field parameter decay the velocity gradient. As a result, it is important to note that when the thermal radiation and Brownian motion variables concurrently escalate, the temperature fields intensify noticeably. The concentration gradient increased with the intensification values of the solutal Biot number and Brownian movement. Additionally, the local density number, heat, and mass transfer rates are computed. A tabulated evaluation of the present findings with outcomes in the research in the limited situation is performed to demonstrate the precision of the chosen numeric approach.

Keywords: Bioconvection flow, Chemical reaction, Curved surface, Magnetised flow, Nanofluid, Thermal radiation

Introduction

Bacterial movement creates gradients of density during bioconvection due to the flow of mixed microbes or biological solutions inside diluted liquids. The motion of unicellular bacteria is the main cause of instability. On the other hand, microbial suspensions cause hydrodynamic instability in nanofluids, which display similar instability features because of nanoscale mobility. This contrast draws attention to the possibility of notable changes in evaporation processes when microbes are added to nanofluids. Kuznetsov *et al.*[1] addressed the stabilization of nanoparticles comprising microorganisms. Moradi *et al.*[2] suggested the impact of the magnetic field on the buoyancy bioconvection flow of nanomaterial upon stretchy surface. Khan *et al.*[3] considered the significance of the time-dependent microorganism flow of magnetized nanomaterial through a stretchable surface. Wu *et al.*[4] elaborated the irreversible bioconvection tangent hyperbolic nanomaterial subject to the heated radiation and first order chemical factor. Hussain *et al.* [5] described the chemical species of microorganisms for the nanoliquid, considering carbon nanotube. Rana *et al.* [6] explained the steady axisymmetric flow of the bioconvection uniform cone disk using numerical simulation. Galal *et al.*[7] explored the bioconvection flowin the nanoliquid of viscoelastic model past a stretchable cylinder with Lorentz force applied. Gasmi *et al.* [8] discovered the impact of magnitised bioconvection non-Newtonian fluidic upon the disk with the heated radiation. Chaudry *et al.*[9] examined the heated radiative magnetised flow of nanomaterial consisting of microorganisms within a rotatory oscillated disk.

The movement of fluid across a curved surface has numerous potential applications within mechanical engineering and industry, including polymeric evacuation in melting and rotating shapes, efficient

evacuation of sheets of plastic, optical fiber production. Ramzan *et al*.[10] inspected the exploration of heat flux under magnetized flow of nanomaterial upon a curved surface. Nabwey *et al*.[11] scrutinized the thermal exploration of Carreau fluid consisting of three nanoparticles upon an exponentially curved surface. Haq *et al*.[12] computed the magnetic field of the nanomaterial through a machine learning approach and a non-similar solution. Sharma *et al*.[13] debated the influence of homogeneous/heterogeneous reactions upon a heated curved surface with the Lorentz effect. Ibrahim *et al*.[14] illustrated the Boussinesq approximation of radiative flow of hybrid nanoparticles upon stretchable/shrinkable curvy surface using stability solution. Muhammad *et al*. [15] debated the magnetized hybrid nanoliquid upon a curve surface considering numerical solution. Badruddin *et al*.[16] deliberated the impact of heat generation/absorption for the significant of nanoparticle (ZnO-SAE50) upon a lubricating curved surface. Jan *et al*. [17] discussed the mixed convection thermal radiation of tri-hybrid nanoparticles ina non-similar solution upon a curved surface. Rafiq *et al*.[18] reported the computational study of the magnetic field effect on the second fluid upon a surface.

Nanoliquids are substances that are an arrangement of nanomaterials in fundamental materials. These kinds of fluids have numerous applications in scientific, technological, and engineering fields, including vehicular and commercial air conditioning, chemotherapy for cancer, oil extraction, and shock absorption. Choi[19] first proposed the notion of nanoparticle dispersion in a fluid. Buongiorno[20] devised a new model for dispersing nanomaterials in liquids using Brown's law and thermophoresis as methods. These consequences are crucial in addressing mass and heat transportation difficulties. Using the aforementioned model, researchers have explored different ways to fluid flow on various surfaces. Hosseinzadeh *et al*.[21] computed the impact of the exploration of non-Newtonian nanoliquid for the magneto flow upon a curved surface. Pattanaik *et al*. [22] expressed the impact of the chemical factor on the nanoliquid subject to the Darcian Forchheimer flow with heated constraint. Razzaq *et al*.[23] communicated the viscoelastic nanoliquid for the buoyancy force upon an exponentially stretchable surface. Abbas *et al*.[24] manifested the porosity flow of a nanoliquid of viscoelatics slippery surface with a heated source/sink. Waqas *et al*.[25] exhibited the zero mass flux of magento Jeffey nanoliquid upon a movable surface. Basit *et al*.[26] intimated the comparison analysis of radiative flow containing nanoliquid with activated energy along the chemical factor upon a wedge surface. Yasmin *et al*.[27] revealed the numerical solution of magneto Newtonian MgO –water nanoliquid for enclosure fins.

The evaluation of magnetic hydrodynamics (MHD) flow along with heat transportation across a stretching curved surface has gained attention due to its use in modern technological and mathematical methods such as melting and spinning and the cooling of large metal plates, polymers simulation from coloured cardboard and plastic material manufacturing, thermoplastic and rubber sheet manufacturing, rolling paper production, and curve-shaped attachments of stretchable assembly machinery. Mahabaleshwar *et al*.[28] explored the velocity slipping effect for the magnetized flow on the non-Newtonian fluid with heated convective condition upon a shrinkable surface. Alharbi *et al*.[29] discussed the significance of the nanomaterial for the magento flow of non-Newtonian fluid across the slendring surface. Muhammad *et al*.[30] deliberated the influence of Darcy Forchheimer magneto bioconvection flowing relation of nanoparticles via numerical simulation. Hansda *et al*.[31] explained the radiative flow second law analysis magneto-hybrid nanoliquid via wavy cavity surface. Jamrus *et al*.[32] discovered the magneto flow of hybrid nanoliquid with velocity slip effect and stratified via stretchable sheet . Tahir *et al*.[33] explored the magneto flow of ferro nanoparticles containing Mn, Zn and Fe_2O_4 subject stretchable sheet.

This work examined the thermal/solutal affects the magnetised bioconvection flow of a nanofluid across a curved surface. To the best of our knowledge, the above mentioned researchers have not examined bioconvection nanomaterial over a thermal\solutal curve surface. Thermal radiation, chemical reaction and heat generation/absorption have been accounted. Matlab bvp4c function obtained the solution of the converted equations. The physical interpretation are decribed in the graphical and tabular form with various parameters. Our flow model's numerical findings align with earlier research, indicating significant agreement. The findings give novel development concepts towards magnets micro biological reactors, optoelectronic biological sensors, and specific drug delivery techniques using

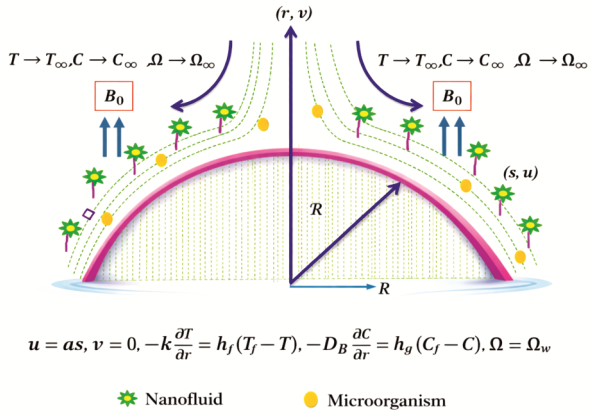

Fig. 1 — Physical flow of the model

thermophilic bacterial strains.The following research question has been given below

- How did nanoscale aggregation influence on the energy and concentration gradient?
- How would be the essential electromagnetic field curve velocity?
- Where may chemical reactions to nanoparticles concentration variations affect airflow distributions?
- Which amount of nanoparticle causes adverse impacts upon microbe movement, denying the biological convection theory?
- How two-dimensional flow variables on drag force, Nusselt number, Sherwood and motile density?

Mathematical Formulation

Consider the incompressible, steady magneto bioconvection flow of nanomaterial thermal radiation effect upon a curved stretchable sheet. The thermal and solutal convective conditions have been used on the curve surface. For descriptions of the framework, employ the curvilinear variables (r, s). Two equivalent but opposed forces within the s position maintain the point of origin static, causing the material to extend around a circular shape of radius R. The $r-$direction is commonly used on the surface. Suppose that the sheet's stretch velocity can be expressed by $u = u_w(s) = as$ and its stretching characteristic is a. Magnetic field strength depicted by $B_0$to the direction of motion r. Additionally, T_f and C_f are the thermal and mass on the curved sheet, and Ω_w is the wall of the surface of the motile density. As r approaches infinity, ambient conditions are denoted by $T_\infty, C_\infty, and\ \Omega_\infty$. The physical model of the bioconvection nanomaterial has been depicted in Fig. 1. The mathematical equations driving a nanofluid that comprise radiation flux and chemical responses can be expressed in the following manner, depending on the presumptions:

$$\frac{\partial v}{\partial r} + \frac{v}{r+R} = -\left(\frac{R}{r+R}\right)\frac{\partial u}{\partial s}, \quad \ldots (1)$$

$$\frac{u^2}{r+R} - \frac{1}{\rho}\frac{\partial p}{\partial r} = 0, \quad \ldots (2)$$

$$v\frac{\partial u}{\partial r} + \frac{uv}{r+R} + \frac{1}{\rho}\frac{R}{r+R}\frac{\partial p}{\partial s} = -\frac{Ru}{r+R}\frac{\partial u}{\partial s} + \nu\left(\frac{\partial^2 u}{\partial r^2} + \frac{1}{r+R}\frac{\partial u}{\partial r} - \frac{u}{(r+R)^2}\right) - \frac{\sigma B_0^2}{\rho}u, \quad \ldots (3)$$

$$v\frac{\partial T}{\partial r} + \frac{Ru}{r+R}\frac{\partial T}{\partial s} = \left(\alpha_f + \frac{16\sigma^* \mathcal{T}_\infty^3}{3k^*(\rho C_p)_f}\right)\left(\frac{\partial^2 T}{\partial r^2} + \frac{1}{r+R}\frac{\partial T}{\partial r}\right) + \tau\left(\frac{D_T}{T_\infty}\frac{\partial^2 T}{\partial r^2} + D_B\frac{\partial C}{\partial r}\frac{\partial T}{\partial r}\right) - \frac{Q^*}{(\rho cp)_f}(T - T_\infty), \quad \ldots (4)$$

$$v\frac{\partial c}{\partial r} + \frac{Ru}{r+R}\frac{\partial C}{\partial s} = D_B\left[\frac{\partial^2 C}{\partial r^2} + \frac{1}{r+R}\frac{\partial C}{\partial r}\right] + \frac{D_T}{T_\infty}\left(\frac{\partial^2 T}{\partial r^2} + \frac{1}{r+R}\frac{\partial T}{\partial r}\right) - Kr(C - C_\infty), \quad \ldots (5)$$

$$v\frac{\partial \Omega}{\partial r} + \frac{Ru}{r+R}\frac{\partial \Omega}{\partial s} = D_m\left[\frac{\partial^2 \Omega}{\partial r^2} + \frac{1}{r+R}\frac{\partial \Omega}{\partial r}\right] - \frac{bW_c}{C_w - C_\infty}\frac{\partial}{\partial r}\left(\Omega\frac{\partial C}{\partial r}\right). \quad \ldots (6)$$

The symbols u and v signify the $s-and\ r-$ direction. The p describes the pressure, νdescribes the viscosity, σdescribes electrical conductivity, B_0describes magnetic field strength, μ describes dynamics viscosity of fluid, ρdescribes fluid density, (ρC_p)describes heat capacity of nanoparticles, $D_T$describes thermophoresis coefficient, Tdescribes temperature of the fluid, T_f describes temperature of the fluid, C_f describes concentration of the liquid, h_f describes heat transport coefficient, h_g describes mass transport coefficient, b describes chemotaxis constant, D_B describes Brownian motion, $\Omega_w$describes wall of the microorganism, T_∞describes the ambient temperature, Q^* describes heat source/sink, C_∞describes concentration field, Ω_∞ describes ambient microorganism density, W_c describes swimming cell speed, D_m describes living microbes density, σ^* describes Stefan Boltzman constant.

The boundary constraint is [36]

$$\left.\begin{aligned} u = as, v = 0, -k\frac{\partial T}{\partial r} = h_f(T_f - T), \\ -D_B\frac{\partial C}{\partial r} = h_g(C_f - C), \Omega = \Omega_w at\ r = 0 \\ u \to 0, \frac{\partial u}{\partial r} \to 0, T \to T_\infty, C \to C_\infty, \Omega \to \Omega_\infty \text{ as } r \to \infty. \end{aligned}\right\} \ldots (7)$$

The subsequent factors have been included to streamline the equations.

$$\left.\begin{aligned}\xi=\sqrt{\frac{a}{\nu_f}}r, u=asF', v=-\frac{R}{r+R}\sqrt{a\nu_f}F, \Theta(\xi)=\frac{T-T_\infty}{T_f-T_\infty},\\ \Xi(\xi)=\frac{C-C_\infty}{C_w-C_\infty}, \psi(\xi)=\frac{\Omega-\Omega_\infty}{\Omega_w-\Omega_\infty}, p=\rho_f(as)^2p(\xi)\end{aligned}\right\} \quad \ldots (8)$$

The aforementioned transformations (8) match Eq. (1) thus transformed nonlinear PDE's Eqs (2)-(6) into nonlinear ODE's Eqs (9)-(13).

$$p'=\frac{F\prime}{\xi+\epsilon} \quad \ldots (9)$$

$$\left.\frac{2\epsilon}{(\xi+\epsilon)}p=\frac{\epsilon}{(\xi+\epsilon)}FF''-\frac{\epsilon}{(\xi+\epsilon)}F'^2+\frac{\epsilon}{(\xi+\epsilon)^3}FF'\right\} \quad \ldots (10)$$

$$\left(1+\tfrac{4}{3}Rd\right)\Theta''+Pr\frac{\epsilon}{(\xi+\epsilon)}F\Theta'+\frac{\Theta'}{(\xi+\epsilon)}-Pr\Theta Qs+\Theta'\Xi'Nb+\Theta'^2Nt=0 \quad \ldots (11)$$

$$(\Xi'')+\frac{Sc\,\epsilon}{(\xi+\epsilon)}F\Xi'+\frac{\Xi\prime}{(\xi+\epsilon)}-ScCh\Xi+Nt/Nb\Theta''=0 \quad \ldots (12)$$

$$\psi''+\frac{\psi'}{(\xi+\epsilon)}+\frac{Lb\,\epsilon}{(\xi+\epsilon)}F\psi'-Pe\big(\psi'\Xi'+\Phi''(\varpi+\psi)\big)=0 \quad \ldots (13)$$

Eqs (9) and (10) remove the pressure term.

$$F^{iv}+\frac{2}{(\xi+\epsilon)}F'''+\frac{1}{(\xi+\epsilon)^3}F'-\frac{1}{(\xi+\epsilon)^2}F''+\left\{\frac{\epsilon}{\xi+\epsilon}(F'''-F'F'')+\frac{\epsilon}{(\xi+\epsilon)^2}(FF''-F'^2)-\frac{\epsilon}{(\xi+\epsilon)^3}FF'\right\}-MF'=0 \quad \ldots (14)$$

Converted boundary conditions is:

$$\left.\begin{aligned}F(0)=0, F'(0)=1, \Theta'(0)=-\gamma_a\big(1-\Theta(0)\big), \Xi'(0)=\\ -\gamma_b\big(1-\Xi(0)\big), \psi(0)=1\\ .\\ F'(\infty)\to 0, F''(\infty)\to 0, \Theta(\infty)\to 0,\\ \Xi(\infty)\to 0, \psi(\infty)\to 0\end{aligned}\right\} \quad \ldots (15)$$

Here, $\epsilon=R\sqrt{\frac{a}{\nu_f}}$ is the curvature parameter, $M=\varepsilon\sqrt{\frac{a}{\nu_f}}$ is slip variable, $Fr=\frac{C_b}{K^{1/2}}$ is the inertia coefficient, $\lambda=\frac{\nu}{K^*}$ is the porosity variable, $\gamma_a=\frac{h_f}{\kappa_f}\sqrt{\frac{\nu_f}{a}}$ is the Biot number, $\gamma_b=-\frac{h_g}{D_B}\sqrt{\frac{\nu_f}{a}}$, solutal biot number, $Nt=\frac{\tau\,D_T(T_f-T_\infty)}{T_\infty\nu_f}$ is the Brownian motion, $Nb=\frac{\tau\,D_B(C_W-C_\infty)}{\nu_f}$ is the thermophoresis variable, $Rd=\frac{4}{3}\frac{\sigma^*}{\kappa*}\frac{T_\infty^3}{k_f}$ is the radiation parameter, $Pr=\frac{\nu_f(\rho cp)_f}{\kappa_f}$ is the Prandtl number, $Sc=\frac{\nu}{D}$ is Schmidt number.the concentration of microorganisms $\varpi=\frac{\Omega_w}{\Omega_w-\Omega_\infty}$the Peclet number $Pe=\frac{bw_c}{D_m}$, the bioconvection Lewis number $Lb=\frac{\nu_f}{D_m}$.

The following values are also to be noticed

Engineering quantities

The engineering quantities are explained as as[39]

$$\left.C_f=\frac{\tau_{rs}}{\rho_f U_w^2}, Nu_s=\frac{sq_w}{\kappa_f(T_f-T_\infty)},\\ Sh_s=\frac{sq_j}{D_B(C_w-C_\infty)}, Nh_s=\frac{sq_m}{D_m(\chi_w-\chi_\infty)}\right\} \quad \ldots (16)$$

Where τ_{rs} is the shear stress, $q_w, q_j, q_m$are heat, mass and motile density are described as

$$\left.\begin{aligned}\tau_{rs}=\left[\mu_f\left(\frac{\partial u}{\partial r}\right)-\left(\frac{u}{r+R}\right)\right]_{r=0}, q_w=-k\left(1+\frac{16\sigma*T_\infty^3}{3k^*\kappa_f}\right)\left(\frac{\partial T}{\partial r}\right)_{r=0}\\ q_j=-D_B\left(\frac{\partial C}{\partial r}\right)_{r=0}, q_m=-D_m\left(\frac{\partial \chi}{\partial r}\right)_{r=0},\end{aligned}\right\} \quad \ldots (17)$$

Given Eqns. (9,17, 18) we have[39]

$$\left.\begin{aligned}Re_s^{\frac{1}{2}}C_f=\left[F''(0)-\frac{F'(0)}{\delta}\right], Re_s^{-\frac{1}{2}}Nu_s=-\left[1+\frac{4}{3}Rd\vartheta'(0)\right],\\ ,\\ Re_s^{-\frac{1}{2}}Sh_s=-\Phi'(0), Re_s^{-\frac{1}{2}}Nh_s=-\Upsilon'(0)\end{aligned}\right\} \quad \ldots (18)$$

Numerical procedure

The conversion of model ODE's (9-14), along with the boundary condition Eq. (15) have been assigned into new variable. These new variables are considered via the numerical approach bvp4c, implemented in MATLAB. This results in higher-order ODEs, which are subsequently simplified by assigning a new variable. Fig. 2 depicts the flow chart of the numerical computation.

$$\left.\begin{aligned}F=\mathrm{Z}_1, F'=\mathrm{Z}_2, F''=\mathrm{Z}_3, F'''=\mathrm{Z}_4, F^{iv}=\mathrm{Z}_4',\\ \Theta=\mathrm{Z}_5, \Theta'=\mathrm{Z}_5, \Theta''=\mathrm{Z}_5',\\ \Xi=\mathrm{Z}_6, \Xi'=\mathrm{Z}_7, \Xi''=\mathrm{Z}_7'\\ \Omega=\mathrm{Z}_8, \Omega'=\mathrm{Z}_9, \Omega''=\mathrm{Z}_9'\end{aligned}\right\} \quad \ldots (19)$$

$$F^{iv}=[-\frac{2}{(\xi+\epsilon)}\mathrm{Z}_4-\frac{1}{(\xi+\epsilon)^3}\mathrm{Z}_1+\frac{1}{(\xi+\epsilon)^2}\mathrm{Z}_2-\left\{\frac{\epsilon}{\xi+\epsilon}(\mathrm{Z}_4-\mathrm{Z}_2\mathrm{Z}_3)+\frac{\epsilon}{(\xi+\epsilon)^2}(\mathrm{Z}_1\mathrm{Z}_2-(\mathrm{Z}_2)^2)-\frac{\epsilon}{(\xi+\epsilon)^3}\mathrm{Z}_1\mathrm{Z}_2\right\}-M\mathrm{Z}_2] \quad \ldots (20)$$

$$\mathrm{Z}_5'=\frac{-\mathrm{Pr}\frac{\epsilon}{\xi+\epsilon}\mathrm{Z}_1\mathrm{Z}_6-\frac{\mathrm{Z}_6}{\xi+\epsilon}+Pr\mathrm{Z}_4Q-\mathrm{Z}_6\mathrm{Z}_8Nb-Z_6Z_6Nt}{\left(1+\frac{4}{3}Rd\right)} \quad \ldots (21)$$

$$Z_8'=-Sc\frac{\epsilon}{\xi+\epsilon}Z_1Z_8+ScKrZ_8-\frac{Nt}{Nb}Z_6' \quad \ldots (22)$$

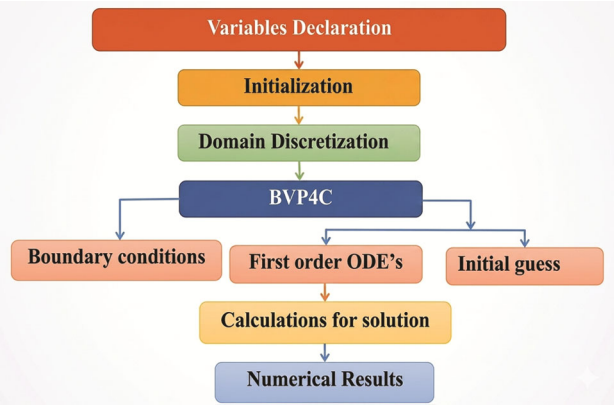

Fig. 2 — Flow chart of numerical method

Table 1 — comparing $C_{fr}(Re_s)^{1/2}$skin friction at the surface for different values of $Fr = 0, \Gamma = 0$

ϵ	Ahmed and Khan[35]	Sanni *et al.*[34]	Current result
10	1.0725	1.0734	1.0731
40	1.0173	1.0176	1.0173
100	1.0034	1.0034	1.0035
1000	1.0007	1.0008	1.0007

$$Z'_{10} = -Lb\frac{\epsilon}{\xi+\epsilon}Z_1Z_{10} - \frac{Z_{10}}{(\xi+\epsilon)} + Pe(Z_{10}Z_8 + Z'_8(\varpi + Z_7)) \quad \text{... (23)}$$

First converted boundary conditions is

$$Z_1(0) = 0, Z_2(0) = 1, Z_4(0) = -\gamma_a(1 - Z_5(0)),$$
$$Z_6(0) = -\gamma_b(1 - Z_7(0)), Z_9(0) = 1$$
$$,$$
$$Z_2(\infty) \to 0, Z_3(\infty) \to 0, Z_5(\infty) \to 0, Z_7(\infty) \to 0, Z_9(\infty) \to 0 \quad \text{... (24)}$$

The ξ_∞ is selected large enough to satisfy the interface restrictions asymptotically. The step size ($\Delta\xi$= 0.0001) and error tolerance (10−8) are carefully adjusted for optimal convergence.

Validated with current result

The precision of the supplied concept needs to be verified. To validate our computational conclusions, we assess numerical information for skin friction (Cfr) in a specific case. The basic viscosity flow of fluid theory is obtained by setting M = 0. Table 1 validates the numerical outcomes from the modeling process and shows that our numerical results are virtually identical to those of the references.

Results and Discussion

This experiment aimed to analyze the magneto-bioconvection flow of viscous nanomaterial past a curved surface. The study focuses on examining the impact of chemical factor, thermal radiation and heat generation/absorption, especially considering thermal/solutal convective applied on the boundary condition. The various physical interpretations have been examined through velocity factor $F'(\xi)$, thermal gradient $\Theta(\xi)$, mass gradient $\Xi(\xi)$, and motile microorganism distribution $\Omega(\xi)$. The explanation of various flow variables is plotted in Figs 3-8. The engineering quantities, radial drag force, heat, mass, and motile microbes are computed through Table 2-5.

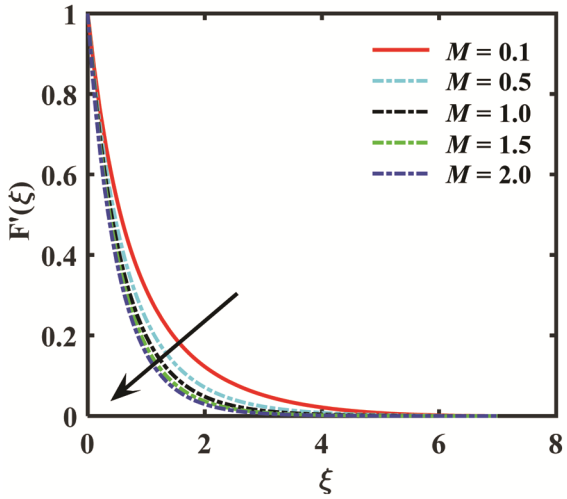

Fig. 3 — Plot of M against $F'(\xi)$

Fig. 3 evaluates the influence of the magnetic field (M) upon the velocity gradient $F'(\xi)$. Applying the magnetic field factor substantially declines the velocity gradient. If a magnet is introduced to an electrically flowing substance, it generates a current of electricity. The generated flow combines against the magnetic field, producing a Lorentz effect. Additionally, the force of Lorentz operates along the contrary orientation of the liquid's velocity, similar to a resisting bodily strain.

Fig. 4a examines the consequences of Bownian factor (Nb) across the temperature profile $\Theta(\xi)$. Changing the Nb causes an upward trend in temperature near the surface. Brownian movement phenomenon enables nanocrystals to shift randomly through large regions to small regions. This erratic movement improves nanoscale transfer of energy because of multiple collisions among nanocrystals with aqueous particles. As a consequence, additional heat is transferred throughout the medium. Fig. 4b views the influence of thermophoretic force (Nt) upon $\Theta(\xi)$. Greater estimation of Nt elevates the

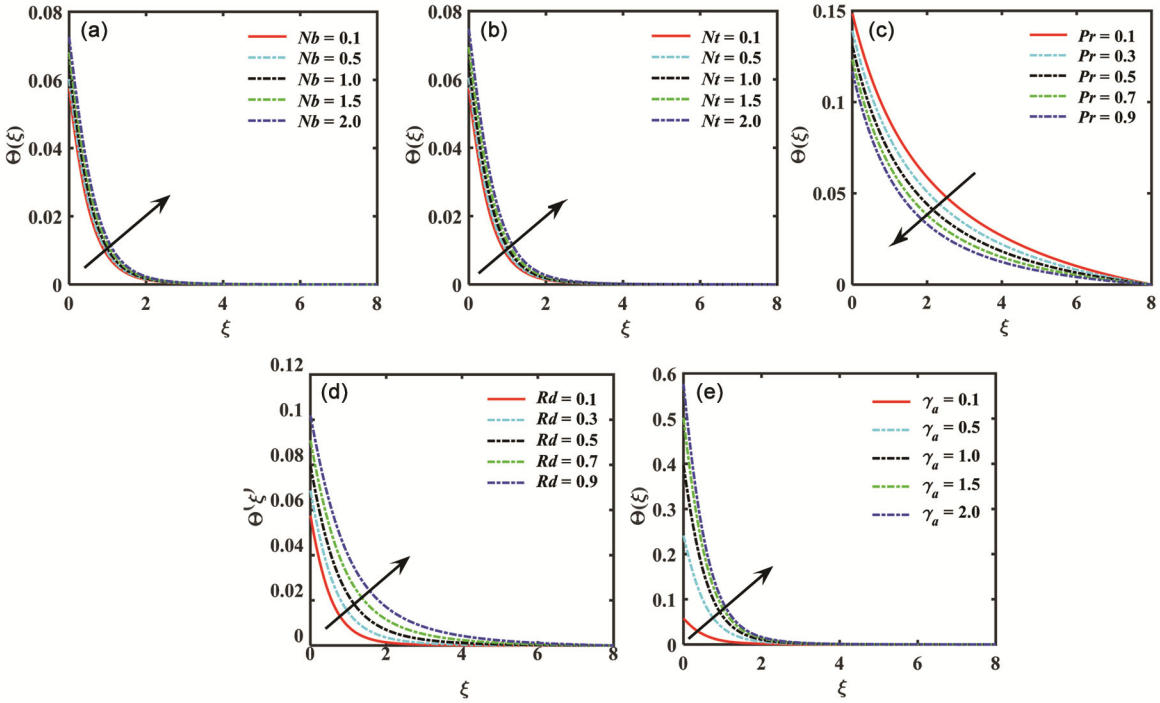

Fig. 4 — Plot of (a) Nb, (b) Nt, (c) Pr, (d) Rd and (e) $\gamma_a$against $\Theta(\xi)$.

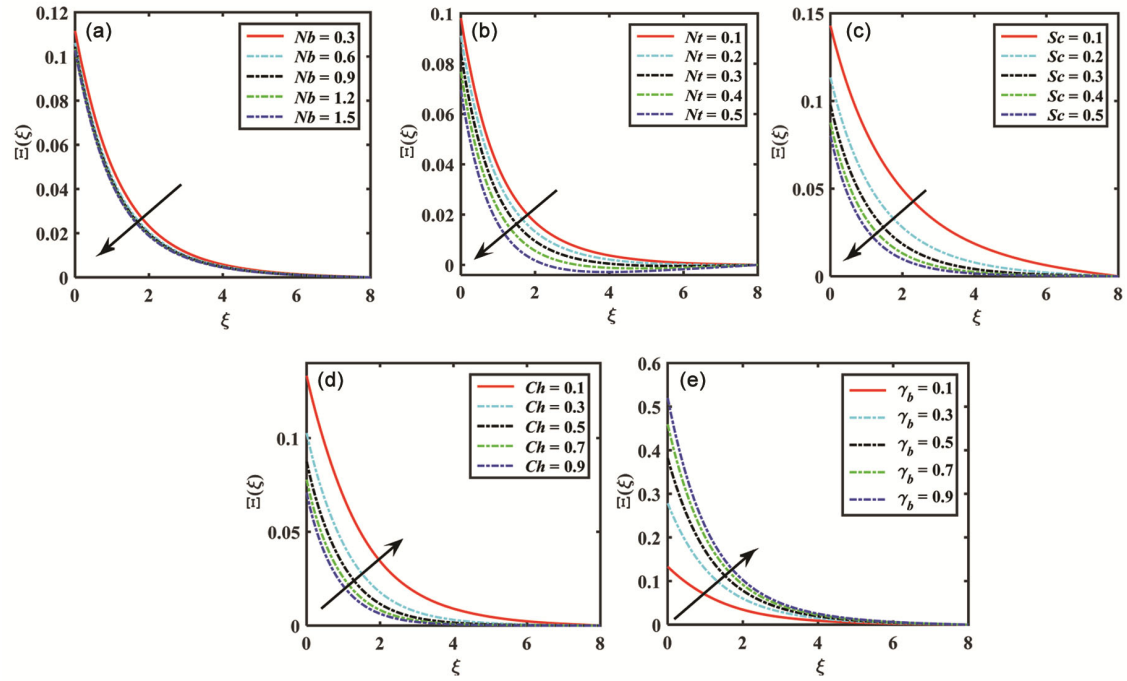

Fig. 5 — Plot of (a) Nb, (b) Nt, (c) Sc, (d) Ch and (e) $\gamma_b$against $\Xi(\xi)$

$\Theta(\xi)$ value. The heating process moves nanomaterials away from the heating substrate and against the less warm diffuse fluid. The particle motion transports heat through the heated barrier to the liquid domain. Fig. 4c illustrates the impact of Prandtl number (Pr) upon $\Theta(\xi)$. When the Pr boosts, the thermal gradient diminishes. An elevated Pr indicates liquids that have poor thermal diffusion.

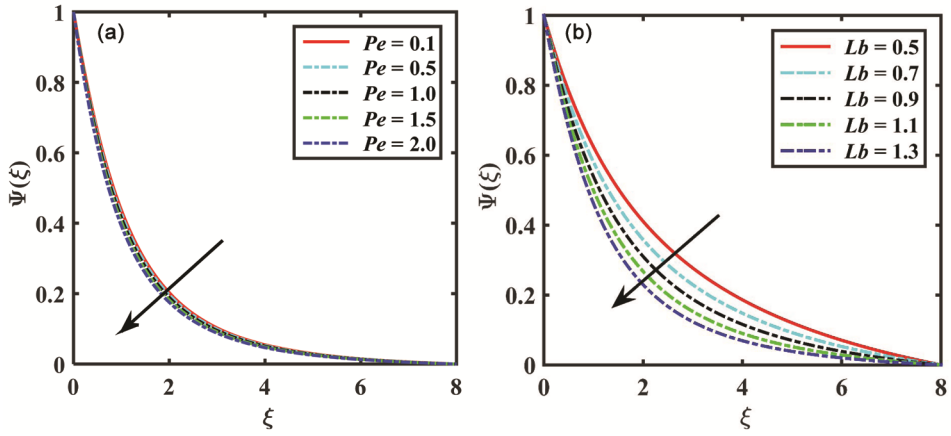

Fig. 6 — Plot of (a) Pe and (b) Lb against $\psi(\xi)$

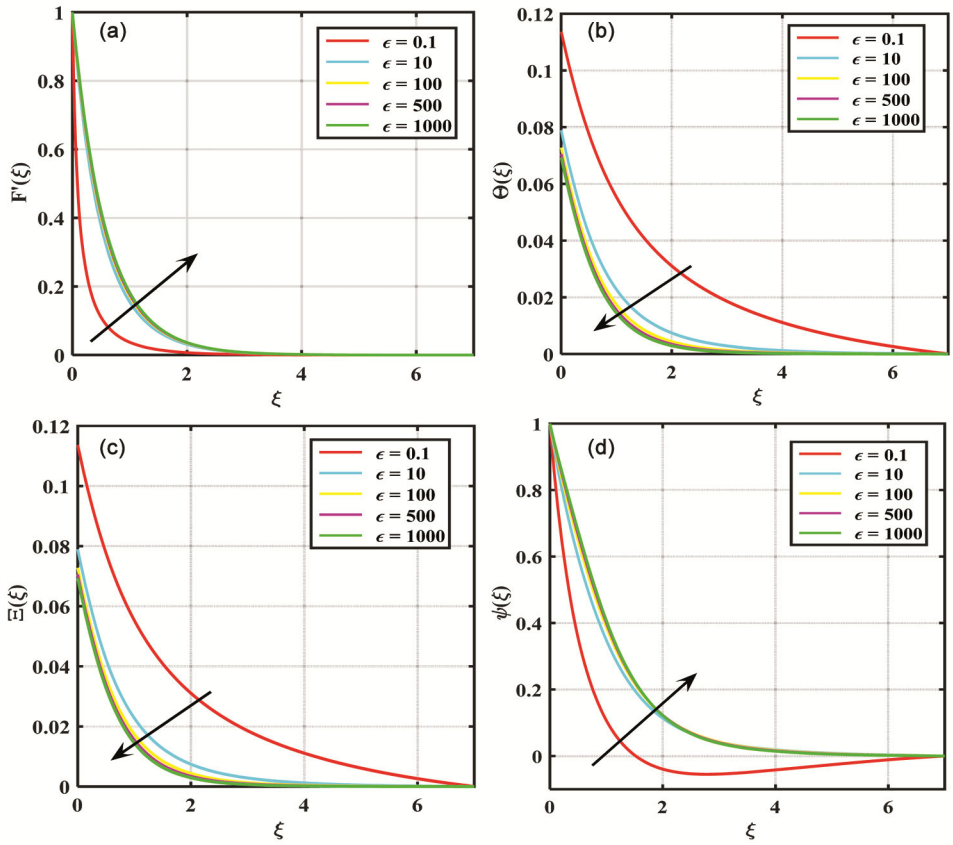

Fig. 7 — Plot of ϵ against (a) $F'(\xi)$, (b) $\Theta(\xi)$, (c) $\Xi(\xi)$ and (d) $\psi(\xi)$

Fig. 4d demonstrates the significance of thermal radiation upon $\Theta(\xi)$. A bigger estimation of the thermal radiation parameter (Rd) elevates the temperature gradient. In alongside conductive over convective, thermal radiation provides another mechanism for thermal movement. Radiant heat flow increases the transfer of energy via the heating substrate to the fluid. This phenomenon enhances the liquid's diffusion properties. Fig. 4e explains the analysis of the Biot number (Bi) across $\Theta(\xi)$. Higher Bi numbers boost the heating of the surface. When Bi grows, the heat exchange among its outermost layer with the fluid that surrounds gets more effective over convective. This improves the thermal supply through the exterior wall to the liquid, causing a shift in the ambient temperature gradient.

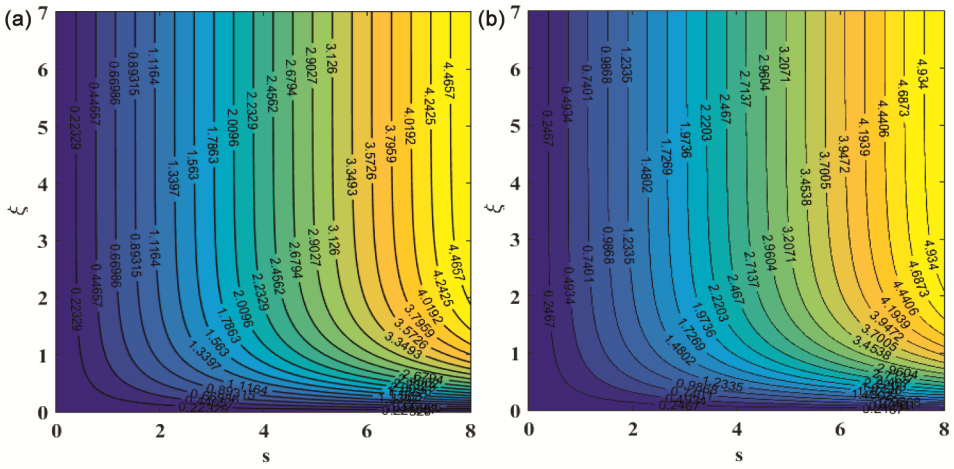

Fig. 8 — Plot of streamline with (a) $M = 0.1, \epsilon = 0.3$ and (b) $M = 0.4, \epsilon = 1.3$

Table 2 — Performance of Drag force against numerous involved physical parameters

ϵ	M	$-Re_s^{1/2}C_f$
3.0	1.0	5.4049
4.0		4.5026
5.0		4.1385
6.0		3.9620
	1.1	2.3299
	1.2	2.3647
	1.4	2.4197
	1.7	2.4642

Table 3 — Performance of Nusselt number against numerous involved physical parameters

γ_a	Rd	Qs	Nb	Nt	ϵ	$Re_s^{-1/2}Nu_s$
0.2	0.1	1.1	0.4	0.6	0.2	0.4467
0.3						0.4546
0.4						0.4672
0.5						0.4798
	0.3					0.5577
	0.5					0.6679
	0.8					0.7781
	0.9					0.8881
		0.1				0.1356
		0.5				0.4320
		1.0				0.6354
		1.5				0.8962
			0.6			0.6770
			0.8			0.7145
			1.2			0.7507
			1.4			0.7853
				0.9		0.5617
				1.2		0.6007
				1.4		0.6411
				1.7		0.6832
					0.2	0.1098
					0.5	0.1121
					0.7	0.1982
					0.9	0.2871

Fig. 5a reveals the importance of the Brownian motion (Nb) and the concentration gradient $\Xi(\xi)$. A spike in Nb minimizes nanoscale deposition over the outer layer. When Nb levels rise, the erratic mobility of nano accelerates, accelerating the diffusion of mass out of its outermost layer. Fig. 5b exemplifies the thermophoretic force (Nt) over $\Xi(\xi)$. Whenever Nt grows, higher thermophoretic pressures drive nanoscale particles far towards the hot barrier and toward a cooler liquid area. The outcome is an augmentation of a concentration gradient. Fig. 5c depicts the insight of Schmidt number (Sc) over $\Xi(\xi)$. Increasing Sc numbers inhibit the diffusion of molecules, causing the particular species to stay near to the wall. Thus, the concentration declines with larger values of Sc. Fig. 5d highlights the features of a chemical reaction (Ch) against $\Xi(\xi)$. Boosting the chemical response factor reduces the concentration field. Fig. 5e illustrate the influence of solutal Biot number on the concentration gradient, boosting concentration filed due to larger magnitude of solutal Biot number.

Fig. 6a elucidates the variation of microorganism density $\psi(\xi)$ with augmenting values of Peclet number (Pe). Convection transportation takes precedence over microbial migration when Pe rises. The microbe's density pattern diminishes as a consequence of the microorganisms being carried along with the movement of water. Fig. 6b describes the fluctuation of $\psi(\xi)$ with augmenting values of Bioconvection Lewis number (Lb). Convection

Table 4 — Performance of Sherwood number against numerous involved physical parameters

γ_b	Ch	Nb	Sc	Nt	$Re_s^{-1/2}Sh_s$
0.1					0.7107
0.2					0.7393
0.3					0.7628
0.4					0.7824
	1.3				0.2701
	1.5				0.2493
	1.7				0.2321
	1.9				0.2176
		0.1			0.2772
		0.7			0.28729
		1.3			0.2977
		1.9			0.3031
			1.1		0.3317
			1.3		0.3075
			1.6		0.2873
			1.8		0.2701
				0.5	0.2435
				1.0	0.3565
				1.5	0.3878
				2.0	0.4235

Table 5 — Performance of microorganism against numerous involved physical parameters

ϵ	Lb	Pe	ϖ	$Re_s^{-\frac{1}{2}}Nn_s$
0.1				2.3212
0.2				1.7212
0.5				1.1567
0.7				0.7678
	1.1			1.7621
	1.3			1.7232
	1.5			1.6690
	1.9			1.6076
		1.1		1.3087
		1.2		1.8710
		1.6		2.1391
		1.8		2.8781
			1.1	2.1781
			1.3	2.8719
			1.5	3.8541
			1.9	4.7611

transportation takes precedence over microbial dispersion when Lb rises. The microbe density reduction results from the microorganisms being carried along with the flow.

The variation of curvature variable ($\epsilon = 0.1,10,100,500,1000$) on the velocity gradient $F'(\xi)$ has been seen in Fig. 7a. Formally, a bigger parameter for curvature translates into a greater surface radius, thereby lowering the surface's barrier, which enables the liquid's molecules to travel freely. As a result, motion dissipation grows stronger, allowing greater speeds to escape the substrate. Fig. 7b depicts the significance of the curvature variable (ϵ) upon the temperature field. Greater estimation of the curvature variable decreases the temperature field. In nature, larger curved improves geometrical stretch for base compactness while increasing the transfer of heat across the outside to the surrounding fluid. Fig 7c discusses the impact of curvature variable ($\epsilon = 0.1,10,100,500,1000$) over concentration gradient. When ϵ grows to 10, 100, 500, 1000 the concentration curves drop more rapidly and reach the ambient state lessen estimation of ξ. Physically, larger curving improves interface compactness and geometrical consequences, which increase heat dispersion from the surface into the fluid while decreasing thermal energy retention along the wall. Fig. 7d reveals the impact of the curvature variable on the microbes density gradient $\psi(\xi)$. The larger the estimation of the ϵ enhances the motile microbes.

Fig. 8 explain the streamline pattern for the M and curvature variable. The curved factor improves stream intricacy via generating centrifugal movements including streamlined stretching, but the field of magnets variable maintains the movement by preventing movement. The streamlined designs thus represent an equal amount of geometrical force curvature with magnetic dampening (an electromagnetic field). It is particularly relevant for systems involving mechanically heated pumping, curving tube exchangers, particularly magnetically conducting tiny liquids over surfaces that curve.

Table 2 depicts the fluctuation of the dimensional drag via the magnetic parameter (M) along curvature factor (ϵ). Growing the curvature factor about ($\epsilon = 3.0\ to\ 6.0$) leads for a continuous drop in C_{fs}(5.4049 to 3.9620). This pattern of conduct suggests that increased curvature lessens shear rate.When M = 1.1 to 1.7 the magnetic parameter causes a progressive increase in C_{fs}(2.3299 to 2.4642). The current pattern is linked to the intensification of the Lorentz force, that opposes fluid movement thus generates shear strain near the outer layer, growing shear rate.

Table 3 views the significane of flow variable such as Biot number (γ_a), thermal radiation (Rd), heat

source variable (Qs), Brownian motion variable (Nb), thermophoretic variable (Nt), and Brownian motion variable (ϵ) across the heat rate near the curve surface. Each of the the flow variable investigated had an advantageous effect on the surface heat transport.

Table 4 reveals the mass rate of the flow variables on the Biot number (γ_b), chemical reaction (Ch), Brownian motion (Nb), Schmidt number (Sc) and thermophoresis number (Nt). Greater estimation of Nb, γ_b, Nt, Ch enhances in Sh_s but results in a reduction in Sc.

Table 5 found that the microbe density numberon the microorganism difference variable (ϖ) Peclet number (Pe) are the primary elements that improve microorganism transport, while Bioconvection Lewis number (Lb) and curvature variable (ϵ).

Conclusion

This study examines curved surfaces in relation to bioconvection nanoliquid. This study identifies crucial elements such as magnetic field, thermal radiation and chemical reaction. Additional elements to consider are thermal and solutal convective conditions. The study aims to understand the complex interactions involving water flow variables and their fundamental mechanisms of action. The model simulates viscous fluid flow under realistic temperature and mass conditions, utilizing an external magnetic field and heat generation with spatial variation. This study explores the effects of magnetic forces, microorganisms, thermal radiation, and chemical reactions on thermal systems, including cooling, drug administration, and materials processing. The primary assumptions are:

- Increasing the magnetic field variable declines the velocity field.
- The temperature gradient intensified due to the larger values of Brownian motion, thermophoresis and thermal radiation.
- Bigger values of solutal Biot number and thermophoresis augment the mass gradient while opposite trends are noted for the Brownian motiona and chemical reaction .
- Motile microorganism density declines with the larger values of bioconvection Lewis number and Peclet number .
- Curvature variable enhances the velocity gradient and motile density number but reduction in temperature and concentration fields. As the magnitude of curvature variable increases, the curve becomes a flat surface.

This study sheds fresh light upon linked electromagnetic radiation and biological convection; nonetheless, numerous limitations must be acknowledged. The simulation requires:

- a singular-phase consistent nanofluid in efficient characteristics, neglecting nanoparticle formation as well as sliding.
- microbes that are gyrotactic in uniform movement parameters while disregarding additional taxicab actions as well as nanoparticle-biological relationships.
- the aesthetically thick substance over the radiation simulation.

Conflict of Interest

The authors declare no conflict of interest.

Symbols	Description	Unit
γ_a	Thermal convective parameter	(-)
γ_b	Solutal convective parameter	(-)
ϵ	Curvature variable	(-)
Rd	Radiation parameter	(-)
M	Magnetic filed	(-)
Nb	Brownian motion	(-)
Sc	Schmidt number	(-)
Pr	Prandtl Number	(-)
F'	Dimensionless velocity	(-)
K^*	Mean Absorption	(-)
R	Distance	(-)
Nt	Thermophoresis force	(-)
Θ	Dimensionless temperature field	(-)
ch	Chemical reaction	(-)
Ξ	Dimensionless concentration field	(-)

ψ	Dimensionless microorganism field	(-)
τ	The ratio of effective heat capacity	Dimensionless
Kr	Chemical reaction	Dimensionless
Pe	Peclet number	Dimensionless
Lb	Bioconvection Lewis number	Dimensionless
ϖ	Microorganism concentration difference	Dimensionless
Cf	Skin friction coefficient	Dimensionless
Nu_s	Nusselt number	Dimensionless
Sh_s	Sherood number	Dimensionless
Nh	Motile denisty	Dimensionless
$u, v,$	Component of velocity	ms^{-1}
c_p	Specific heat	$\mathrm{J(kg)^{-1}K^{-1}}$
g	Acceleration due to gravity	ms^{-2}
v_f	Kinematic viscosity	m^2s^{-1}
v_f	Kinematic viscosity	m^2s^{-1}
k	Thermal conductivity	$kgmK^{-1}s^{-3}$
α_f	Thermal diffusivity	m^2s^{-1}
ρ_f	Density of nanofluid	kgm^{-3}
T_∞	Ambient temperature	K
D_B	Brownian diffusion coefficient	m^2s^{-1}
Ω_∞	Ambient concentration of microorganisms	$kg(m)^{-3}$
q_r	Radiative heat flux	$W(m)^{-2}$
σ^*	Stefan-Boltzmann constant	$Wm^{-1}K^{-1}$
T	The temperature of the fluid	K
h_f	Coefficient of heat transfer	$Wk^{-1}m^{-2}$
T_f	Surface heat	K
μ_f	Dynamic visocity	$kg(ms)^{-1}$
α_f	Thermal diffusivity	m^2s^{-1}
D_T	Thermophoretic diffusion coefficient	m^2s^{-1}
Ω_w	Surface concentration of microorganisms	$kg(m)^{-3}$
D_M	Microoganisim diffusion coefficient	m^2s^{-1}
ρ_m	The density of microorganism particles	kgm^{-3}

References

1 Kuznetsov A V, The onset of nanofluid bioconvection in a suspension containing both nanoparticles and gyrotactic microorganisms, *Int Commun Heat Mass Transf*, 37 (2010) 1421.

2 Moradi M R, Hosseinzadeh K, Hasibi A & Ganji D D, Hydrothermal study on nano-bioconvective fluid flow over a vertical plate under the effect of magnetic field, *Numer Heat Transf Part B Fundam*, 85 (2023) 469.

3 Khan M R, Puneeth V, Alaoui M K & Almagrabi A O, Numerical simulation of unsteady MHD bio-convective flow of viscous nanofluid through a stretching surface, *Case Stud Therm Eng*, 53 (2023) 103830.

4 Wu Y, Chaudhry M, Maqbool N, Tahir M, Basit M A & Imran M, Entropy generation in radiative motion of tangent hyperbolic nanofluid in the presence of gyrotactic microorganisms and activation energy, *Front Phys*, 12 (2024) 1.

5 Hussain A, Raiz S, Hassan A, Hassan A, Elhag S H, Alam M M, Hassan A M, Hassan A M & Zardi H, Consequences of higher order chemical reaction on bioconvective carbon nanotubes flow implementing Buongiorno's model, *Kuwait J Sci*, 51 (2024) 100248.

6 Rana P & Basavarajappa M, Bioconvection dynamics in rotating and stationary cone-disk systems, *Phys Fluids*, 36 (2024) 112038.

7 Galal A M, Zeemam M, Imran M, Basit M A, Tahir M, Akram S & Younis J, Numerical exploration of bioconvection in optimizing nanofluid flow through heated stretched cylinder in existence of magnetic field, *Multidiscip Model Mater Struct*, 21 (2024) 425.

8 Gasmi H, Obalalu A M, Akindele A O, Salaudeen S A, Khan U, Ishak A & Abed A M, Thermal performance of a motile-microorganism within the two-phase nanofluid flow for the distinct non-Newtonian models on static and moving surfaces, *Case Stud Therm Eng*, 58 (2024)104392.

9 Chaudhry M, Imran M, Raza M & Idrees N, Thermal and flow analysis of MHD nanofluid between oscillating discs with motile microorganisms: Application in rotating bioreactors, *Case Stud Therm Eng*, 73 (2025) 106459.

10 Ramzan M, Shahmir N, Ghazwani H A S, Elmasry Y & Kadry S, A numerical study of nanofluid flow over a curved surface with Cattaneo-Christov heat flux influenced by induced magnetic field, *Numer Heat Transf Part A Appl*, 83 (2022) 197.

11 Nabwey H A, Rashad A M, Khan W A, El-Kabeir S M M & Abd-Elnaem S, Heat transfer in MHD flow of Carreau ternary-hybrid nanofluid over a curved surface stretched exponentially, *Front Phys*, 11 (2023) 1.

12 Ul-Haq S, Tanveer A, Ashraf M B & Nawaz R, Artificial neural network (ANN) analysis of non-similar solution of

MHD nanofluid flow past a curved stretching surface, *Numer Heat Transf Part A Appl*, 86 (2023) 2399.
13 Sharma R P, Sharma A & Mishra S R, Illustration of homogeneous–heterogeneous reactions on the MHD boundary layer flow through stretching curved surface with convective boundary condition and heat source, *J Therm Anal Calorim*, 148 (2023) 12119.
14 Ibrahim W & Gizewu T, Stability analysis of dual solutions for mixed convection and thermal radiation with hybrid nanofluid flow past shrinking/stretching curved surface, *Sci Rep*, 13 (2023) 21676.
15 Muhammad K, Ahmed B, Sharaf M, Afikuzzaman M & Az-Zo'bi E A, Multiscale tribology analysis of MHD hybrid nanofluid flow over a curved stretching surface, *Nanoscale Adv*, 6 (2023) 855.
16 Shilpa B, Badruddin I A, Reddy R G, Kamangar S & Khan A A, Exploration of linear and exponential heat source/sink with the significance of thermophoretic particle deposition on ZnO-SAE50 nano lubricant flow past a curved surface, *Case Stud Therm Eng*, 61 (2024) 104883.
17 Jan A, Mushtaq M & Hussain M, Nonsimilar analysis of forced convection radially magnetized ternary hybrid nanofluid flow over a curved stretching surface, *Numer Heat Transf Part B Fundam*, 86 (2024) 3093.
18 Rafiq M, Kamran M, Ahmed N, Mohyud-Din S T, Bashir Y, Haider S A, Farwa S & Tahir M, Analytical solution for the flow of second grade fluid over a stretching sheet, *AIP Adv*, 9 (2019) 055313.
19 Choi S U S, Enhancing thermal conductivity of fluids with nanoparticles, *ASME Fluids Eng Div*, (1995) 99.
20 Buongiorno J, Convective transport in nanofluids, *J Heat Transf*, 128 (2005) 240.
21 Hosseinzadeh K, Mardani M R, Paikar M, Hasibi A, Tavangar T, Nimafar M, Ganji D D & Shafii M B, Investigation of second grade viscoelastic non-Newtonian nanofluid flow on the curve stretching surface in presence of MHD, *Results Eng*, 17 (2022) 100838.
22 Pattanaik P C, Jena S, Mishra S R, Alshehri M & Shah N A, Illustration of convective boundary conditions on the darcy-forchheimer flow of nanofluid with the impact of chemical reaction, *Symmetry*, 15 (2023) 1728.
23 Razzaq R, Farooq U & Mirza H R, Nonsimilar forced convection analysis of maxwell nanofluid flow over an exponentially stretching sheet with convective boundary conditions, *ZAMM - J Appl Math Mech / Zeitschrift Für Angewandte Mathematik Und Mechanik*, 103 (2023) 1.
24 Abbas W, Megahed A M, Ibrahim M A & Said A A M, Non-newtonian slippery nanofluid flow due to a stretching sheet through a porous medium with heat generation and thermal slip, *J Nonlin Math Phys*, 30 (2023) 1221.
25 Waqas M, Khan U, Zaib A, Ishak A, Siddiqui M I H & Madhukesh J K, Two-phase numerical simulation of thermal and solutal transport of zero mass flux conditions over a porous deformable disc: The extension of Jeffrey-Hamel model, *Appl Therm Eng*, 250 (2024) 123497.
26 Basit M A, Bashir M M, Imran M, Tahir M, Alharthi A M, Ching D L C & Khan I, Analysis of efficient partial differential equations model for nano-fluid flow through wedge involving minimal energy and thermal radiation, *J Radiat Res Appl Sci*, 18 (2025) 101331.
27 Yasmin S, Khan S A, Fatima N, Imran M, Tahir M, Waqas H, Farooq U & Xu Y J, Computational analysis of MHD MgO-water nanofluid flow inside hexagonal enclosure fitted with fins, *Case Stud Therm Eng*, 43 (2023) 102788.
28 Mahabaleshwar U S, Vanitha G P, Pérez L M & Manca O, An MHD flow of non-Newtonian fluids with CNTs and heat transfer across a linearly shrinking sheet with slip and Biot number, *J Magn Magn Mater*, 577 (2023) 170764.
29 Alharbi K A M, Bilal M, Ali A, Eldin S M, Alburaikan A & Khalifa H A E W, Significance of gyrotactic microorganisms on the MHD tangent hyperbolic nanofluid flow across an elastic slender surface: Numerical analysis, *Nanotechnol Rev*, 12 (2023).
30 Hansda S, Hussein A K, Majhi D, Soren S, Khan U, Al-Sharify Z T & Abdulameer S F, Thermal radiation induced entropy generation in hybrid nanofluid convection under magnetic field in a wavy cavity with localized thermosolutal sources, *J Radiat Res Appl Sci*, 18 (2025) 101845.
31 Jamrus F N, Waini I, Khan U & Ishak A, Effects of magnetohydrodynamics and velocity slip on mixed convective flow of thermally stratified ternary hybrid nanofluid over a stretching/shrinking sheet, *Case Stud Therm Eng*, 55 (2024) 104161.
32 Tahir H, Khan U, Din A, Chu Y M, Muhammad N & Li X M, Hybridized two phase ferromagnetic nanofluid with $NiZnFe_2O_4$ and $MnZnFe_2O_4$, *Ain Shams Eng J*, 12 (2021) 3063.
33 Ashfaq M, Hajlaoui K, Glili I E, Foukhari Y, Arif M, Shah R A, Alrasheedi N H & Khedher N B, Heat and mass transfer analysis of MHD boundary layer flow with motile microorganisms over porous surfaces under variable wall thermal conditions, *Therm Sci Eng Prog*, 66 (2025) 104056.
34 Sanni K M, Asghar S, Jalil M & Okechi N F, Flow of viscous fluid along a nonlinearly stretching curvedsurface, *Results Phys*, 7 (2017) 1.
35 Ahmad L & Khan M, Importance of activation energy in development of chemical covalent bonding in flowof Sisko magneto-nanofluids over a porous moving curved surface, *Int J Hydrog Energy*, 44 (2019) 10197.
36 Khan S A, Imran M, Tahir M, Alhushaybari A, Ching D L C & Khan I, Thermal radiation influence on nodal/saddle stagnation point flow with convective heat transfer in hybrid nanofluids containing gold and zinc nanoparticles, *J Radiat Res Appl Sci*, 18 (2025) 101637.